Activated Pancreatic Stellate Cells Sequester CD8+ T-Cells to Reduce Their Infiltration of the Juxtatumoral Compartment of Pancreatic Ductal Adenocarcinoma

Abasi Ene-Obong[1], Andrew J. Clear[2], Jennifer Watt[1,4], Jun Wang[3], Rewas Fatah[2], John C. Riches[2], John F. Marshall[1], Joanne Chin-Aleong[5], Claude Chelala[3], John G. Gribben[2], Alan G. Ramsay[2], Hemant M. Kocher[1,4]

Centres for [1]Tumour Biology, [2]Hemato-Oncology & [3]Molecular Oncology, Barts Cancer Institute, Barts and The London School of Medicine and Dentistry, Queen Mary University of London, London EC1M 6BQ, UK; Departments of [4]Surgery and [5]Pathology, Barts and the London HPB Centre, The Royal London Hospital, Barts Health NHS Trust, London, E1 1BB, UK.

SUPPLEMENTARY MATERIAL

Supplementary tables

Supplementary table 1: Pancreatico-biliary diseases: patient numbers on respective TMAs

Pancreatico-biliary disease	Number of patients		
	Batch A	Batch B	Total
Ampullary carcinoma	0	9	9
Cholangiocarcinoma	9	12	21
Chronic pancreatitis	0	4	4
Mucinous cystic neoplasm	0	6	6
Normal	0	14	14
PDAC (resected)	63	0	63
PDAC (biopsy)	0	35	35
Total	72	80	152

Supplementary table 2: Pancreatico-biliary diseases: patient characteristics

Diagnosis	n	Age: median (IQR)	Sex M:F	Tumor stage T (n)	Nodal metastasis stage N (n)
Ampullary carcinoma	9	63 (58-79)	4:5	T1 (0), T2 (3), T3 (6), T4 (0)	N0 (2), N1 (7)
Cholangiocarcinoma	21	61 (55-76)	13:8	T1 (0), T2 (6), T3 (13), T4 (0)	N0 (2), N1 (19)
Chronic pancreatitis	4	55 (44-64)	4:0	NA	NA
Mucinous cystic neoplasm	6	48 (40-64)	0:6	NA	NA
Resected PDAC	63	66 (60-77)	30:33	T1 (6), T2 (22), T3 (25), T4 (0)	N0 (24), N1 (39)
Advanced PDAC	35	67 (61-78)	20:15	NA	NA

NA: Not applicable

Supplementary table 3: Details of antibodies used in immunohistochemistry (IHC), immunofluorescence (IF) and flow cytometry

Primary antibody	Species raised in	Supplier	Dilution - IHC
CD3 (clone SP7)	Rabbit	Labvision (CD-3-SP7)	1:500
CD4 (clone 4B12)	Mouse	Novacostra (NCL-CD4-368)	1:500
CD8 (clone C8/144B)	Mouse	Dako (M7103)	1:400
CD20 (clone L26)	Mouse	Dako (M0755)	1:2000
CD56 (clone ERIC-1)	Mouse	Serotec (MCA591)	1:1200
CD68 (clone KP1)	Mouse	Dako (M0814)	1:8000
FoxP3 (clone 263A/E7)	Mouse	Abcam (Ab20034)	1:100
FN (clone FN-3E2)	Mouse	Sigma-Aldrich (F6140)	1:500
Myeloperoxidase	Rabbit	Dako (A0398)	1:8000
CD11b (clone M1/70)	Rat	eBioscience (14-0112)	1:100
Fibronectin	Rabbit	Abcam (ab299)	1:100
F4/80	Rat	eBioscience (14-4801)	1:200
CK (clone OV-TL 12/30)	Mouse	Dako (M701801-2)	1:200
CD8 (clone C8/144B)	Mouse	Dako (M710301-2)	1:50
CD8	Rat	Pierce antibodies (MA1-70041)	1:500
αSMA (clone 1A4)	Mouse	Dako (M085101-2)	1:100
Antibodies	**Species raised in**	**Supplier**	**Dilution - IF**
CD3	Rabbit	Abcam (ab5690)	1:20
CD8	Rabbit	Abcam (ab4055)	1:100
Vimentin (C-20)	Goat	Santa Cruz (sc-7557)	1:100
Alexa Fluor® 488	Goat	Invitrogen (A-11001)	1:2000
Alexa Fluor® 555	Rabbit	Invitrogen (A-21431)	1:100

Antigen retrieval: Heat induced epitope retrieval in pressure cooker using Citrate buffer at pH6.0 for 10 minutes.

Primary antibody (clone)	Species raised in	Supplier (order number)	Conjugate	Gene
CD3 (UCHT1)	Mouse	Biolegend (300419)	PE/Cy7	CD3
CD4 (RPA-T4)	Mouse	eBiosciences (47-0049)	APC-eFlour® 780	CD4
CD8a (RPA-T8)	Mouse	eBiosciences (45-0088)	PerCP-Cy5.5	CD8
CD184 (12G5)	Mouse	BD Pharmingen™ (560936)	APC	CXCR4
CD45RA (H100)	Mouse	BD Pharmingen™ (561882)	FITC	PTPRC
CD197 (3D12)	Rat	eBioscience (12-1979)	PE	CCR7

Supplementary table 4: KPC mice characteristics (all mice had tumor visible on ultrasound before enrolment)

Mouse number	Sex	Age (months)	Treatment
1	F	5	ATRA
2	F	5.75	ATRA
3	F	5	ATRA
4	M	5.5	ATRA
5	M	3	ATRA
6	M	3	ATRA
7	M	7	VEHICLE
8	F	2	VEHICLE
9	F	6.75	VEHICLE
10	F	4.75	VEHICLE

Supplementary Table 5: Survival analyses of immune cell markers in PDAC

MARKER	WHOLE TISSUE INFILTRATE			JUXTATUMOURAL TISSUE INFILTRATE			PANSTROMAL TISSUE INFILTRATE			Inference
	CUT OFF	P-VALUE	Miller-Sigmuend p-value	CUT OFF	P-VALUE	Miller-Sigmuend p-value	CUT OFF	P-VALUE	Miller-Sigmuend p-value	
CD3	<0.12≥	**0.0151**	0.2195	<0.14≥	0.1069	1	<0.20≥	**0.018**	0.2482	↓
CD4	<0.19≥	**0.0069**	0.1217	<0.19≥	0.0652	0.575	<0.16≥	**0.019**	0.2586	↓
CD8	<0.07≥	**0.0302**	0.3555	<0.05≥	**0.0455**	0.4639	<0.09≥	0.0614	0.5553	↑
FoxP3	<0.06≥	**0.0016**	**0.0371**	<0.03≥	**0.0019**	**0.0444**	<0.05≥	**0.0253**	0.316	↓
CD20	<0.00≥	0.0652	0.575	<0.01≥	0.0544	0.5174	<0.05≥	**0.0128**	0.1939	↓
CD56	<0.02≥	**0.0114**	0.1782	<0.03≥	**0.0359**	0.3992	<0.03≥	0.2059	1	↑
CD68	<0.03≥	**0.0269**	0.3288	<0.12≥	0.138	1	<0.02≥	0.1138	1	↓
CD4/CD8	<2.00≥	**0.0455**	0.4639	<3.30≥	0.0783	0.6362	<4.60≥	0.1797	1	↓

Supplementary Figure 1: Immune cell distribution in patients with normal histology, PDAC and cholangiocarcinoma.

Panel shows representative TMA cores from normal pancreas (A, D, G), PDAC patients (B, E, H) and cholangiocarcinoma patients (C, F, I). The cores shown are stained by immuno-histochemistry for H&E (A, B, C), $CD3^+$ T-cells (D, E, F) and $CD8^+$ T-cells (G, H, I).

There are very few $CD3^+$ and $CD8^+$positively staining T-cells in the normal pancreas. In the PDAC cores $CD3^+$ and $CD8^+$T-cells are seen to aggregate in the panstroma, with fewer $CD3^+$ and $CD8^+$positive cells infiltrating the juxtatumoral stroma (J and K). In the cholangiocarcinoma cores $CD3^+$ and $CD8^+$ positive cells are evenly distributed throughout the tissues with no clear difference between the panstromal and juxtatumoral compartments.

The dotted line (J,K) represents the boundary of the juxtatumoral compartment 100 µm margin from the tumor. Scale bars: A- I, 10µm; J-K, 20µm.

Supplementary Figure 2: Double immunostain of CD8/α-SMA and CK/α-SMA on consecutive sections to demonstrate sequestration of $CD8^+$ T-cells in panstromal compartment

Consecutive human tissue sections were doubly stained for $CD8^+$ (brown, DAB)/α-SMA (purple, VIP) (A-D) and CK (brown, DAB)/α-SMA (purple, VIP) (C-G). There is an abundance of $CD8^+$ T-cells in the panstromal compartment seemingly juxtaposed to $\alpha\text{-SMA}^+$ stromal cells (B, D) and few $CD8^+$ cells in the juxtatumoral compartment (C). Cancer cells are absent in the panstromal compartment where $CD8^+$ T-cells are densest (F). Scale bar: 100 µm.

Supplementary Figure 3: Comparison of immune cells density as performed in tissue microarray and whole tissue sections

Immune cells were stained and analyzed as described in Supplementary Figure 1-2.

Immune cell densities (here for $CD8^+$ T-cells) were analyzed on TMAs (A) and whole tissue sections (B) using the Ariol microscope in an automated manner after training for color, shape and size on multiple areas. Box (median with interquartile ranges (25^{th} and 75^{th})) and whisker (5^{th} and 95^{th} centiles) plots demonstrate similar results.

The density of immune cell infiltrate was carried out by two distinct methods: as a proportion of negative (non-stained for the marker: in this case for $FoxP3^+$) cells (C) and as a percentage of all cells (D). Box (median with interquartile ranges (25^{th} and 75^{th})) and whisker (5^{th} and 95^{th} centiles) plots gave same results.

(E) Further analysis of density of immune cells (in this case for $CD68^+$) was given by the stromal compartments were analyzed by dividing the number of positive stained nuclei with the number of negatively stained nuclei to give a proportion of cellular population as in (C) above. (F) Also the positively stained nuclei number was divided by the area in pixels to give an estimate of immune cell density. Each data point represents a single patient (median scores of all TMA cores (n=6)). Both methods gave same results.

N represent the number of patients studied.

Supplementary Figure 4: Immune cell infiltrate in PDAC patients

Panels depict visual comparison of immune cell infiltrate in stromal compartments ('juxtatumoral' defined as within 100µm of tumor and marked by the red dotted line and the rest of the tumor stroma as 'panstromal') for T-cells ($CD3^+$, (A)), helper T-cells ($CD4^+$ (B)) cytotoxic T cells ($CD8^+$, (C)), regulatory T-cells (FoxP3+, (D)), B-cells ($CD20^+$, (E)), natural killer cells ($CD56^+$, (F)), neutrophils ($myeloperoxidase^+$, (G)) and macrophages (CD68+, (H)). Scale bars: 100µm.

Supplementary Figure 5: Stromal compartment specific immune cell infiltration in human PDAC for $CD3^+$ and $CD56^+$ cells.

Comparison of immune cell infiltration in the two PDAC stromal compartments was made for $CD3^+$ (A) and $CD56^+$ (B) as described in Figure 2 and Supplementary Figure 1-2. Each data point represents a single patient (median scores of all TMA cores (n=6)) and lines represent median for the cohort of patients. PDAC tissues demonstrate a significantly lesser density in the juxtatumoral stroma relative to the panstromal compartment for $CD3^+$ and $CD56^+$ cells. Mann Whitney U test; p-values are two-tailed. *** $p< 0.001$; ** $p= 0.001$ to 0.01.

Supplementary Figure 6: Stromal compartment specific immune cell infiltration in an independent cohort of PDAC patients

Immune cells were stained and analyzed as described in Supplementary Figures 1-4. This cohort was formed predominantly by patients with metastatic disease (TMA B). Therefore, these tissues were obtained from biopsy specimens. There is a defect in infiltration of T-cells ($CD3^+$ (A)), helper T-cells ($CD4^+$ (B)) and cytotoxic T cells ($CD8^+$, (C)), and B-cells ($CD20^+$, (E)). In contrast T regulatory cells ($FoxP3^+$ (D)) and macrophages ($CD68^+$ (F)) were not significant, suggesting that these immune cells can access the tumor cells. $CD8^+$ and $CD20^+$ findings are consistent with the primary cohort of patients suggesting that the exclusion of these immune cells from the immediate tumor microenvironment is consistent throughout the disease progression.

Mann Whitney U test; p-values are two-tailed. ** p= 0.001 to 0.01; * p= 0.01 to 0.05.

Number of patients analyzed for each marker are indicated by ‘n’.

Supplementary Figure 7: Stromal compartment specific immune cell infiltration in ampullary cancer patients

Immune cells were stained and analyzed as described in Supplementary Figures 1-4. There was equal infiltrate in the juxtatumoral and pan-stromal compartments of T-cells ($CD3^+$ (A)), helper T-cells ($CD4^+$ (B), cytotoxic T-cells ($CD8^+$, (C)) regulatory T-cells (FoxP3+, (D)) and B-cells ($CD20^+$, (E)) and macrophages (CD68+, (F)). Mann Whitney U test; p-values are two-tailed. N.s: not significant.

Number of patients analyzed for each marker are indicated by 'n'.

Supplementary Figure 8: Stromal compartment specific immune cell infiltration in cholangiocarcinoma patients

Immune cells were stained and analyzed as described in Supplementary Figures 1-4. There was equal infiltrate in the juxtatumoral and panstromal compartments of T-cells ($CD3^+$ (A)), helper T-cells ($CD4^+$ (B), cytotoxic T cells ($CD8^+$, (C)), regulatory T-cells (FoxP3+, (D)) and B-cells ($CD20^+$, (E)) and macrophages (CD68+, (F)).

Mann Whitney U test; p-values are two-tailed. N.s: not significant

Number of patients analyzed for each marker are indicated by 'n'.

Supplementary Figure 9: Correlation of circulating monocytes with CD68$^+$ infiltrate in patients with PDAC.

Correlation plots were constructed for circulating monocytes and the CD68$^+$ immune cell infiltrate in whole tumor-stroma (A) and in distinct stromal compartments: juxtatumoral compartment (B) and panstromal compartment (C) in the PDAC patients. There was no correlation between these counts. Each data point represents one unique patient and the correlation line was plotted as shown with the values representing Pearson's Correlation Coefficient 'r' and the respective p-value.

Supplementary Figure 10: Correlation of circulating lymphocytes with $CD3^+$ infiltrate in patients with PDAC.

Correlation plots were constructed for circulating lymphocytes and the $CD3^+$ immune cell infiltrate in whole tumor-stroma (A) and in distinct stromal compartments: juxtatumoral compartment (B) and panstromal compartment (C) in the PDAC patients There was no correlation between these counts. Each data point represents one unique patient and the correlation line was plotted as shown with the values representing Pearson's Correlation Coefficient 'r' and the respective p-value.

Supplementary Figure 11: Correlation of circulating neutrophils with Myeloperoxidase$^+$ immune cell infiltrate in patients with PDAC.

Correlation plots were constructed for circulating neutrophils and the Myeloperoxidase$^+$ immune cell infiltrate in whole tumor-stroma (A) and in distinct stromal compartments: juxtatumoral compartment (B) and panstromal compartment (C) in the PDAC patients There was no correlation between these counts. Each data point represents one unique patient and the correlation line was plotted as shown with the values representing Pearson's Correlation Coefficient 'r' and the respective p-value.

Supplementary Figure 12: Stromal compartment specific immune cell infiltration in KPC mice treated by vehicle or ATRA.

KPC mice were treated by ATRA or vehicle as earlier described and immunohistochemistry performed for the immune cell markers $CD4^+$ helper T-cells (A), $CD45R^+$ B-cells (B), $F4/80^+$ macrophages (C) and $CD11b^+$ MDSC (D) (quantification for juxtatumoral and panstromal compartments are shown in Figure 4). Juxtatumoral exclusion of $Cd45R^+$ B-cells can be seen in (B). There are no changes in immune cell density for these cells after treatment by ATRA (A-D).

Supplementary Figure 13: Analysis of migration of T-cells

One, four and eight hour durations for migration of T-cells were investigated in order to determine optimal duration required for migration assays. All assays were done in three technical repeats. Various methods for analysis were employed. (A) Absolute $CD3^+$ T-cell numbers that migrated to bottom of Transwell after one, four and eight hours. There was no significance after one hour, however significant differences were observed between activated PSC and quiescent as well as 0% RPMI (without FBS), which served as background, after four and eight hours. (B) Proportion of migrated cells; migrated $CD3^+$ T-cells at the bottom of each well were divided by the total number of cells inserted at beginning of assay. Results are identical to "A" which shows significant differences after four and eight hours.

(C) $CD3^+$ T-cell migration was performed for duration of four hours. RPMI 0% and 10% (FBS) served as background (negative) and positive controls respectively. $CD3^+$ T-cell significantly migrated to RPMI 10% over RPMI 0% and preferentially to activated PSC over 0% and 10% RPMIs. (D) Background migration (RPMI 0%) cell count was deducted from all assay readouts as in "C" to give relative migration; activated PSC remained significant over RPMI 10%. (E) Normalization of "D" to basal migration (RPMI 10%) gave identical results to "D" but allowed comparison across biological repeats carried out from T-cells from different healthy and diseased donors. All data in figures 5 and 7 are presented as amalgamation of these biological repeats from a number of patients/donors.

*** $p< 0.001$. Paired T-test or ANOVA as appropriate.

Supplementary Figure 14: Heatmap of gene expression changes after treatment of PSC with ATRA. (A) Heatmap of gene expression changes for significantly differentially expressed genes involved in cell adhesion (GO:0007155, gene set enrichment test adjusted $p = 0.06$), derived from the ATRA – control time course experiment. Hierarchy clustering of samples from 10 groups, ATRA 30 minutes, 4 hours, 12 hours, 24 hours and 168 hours, as well as control 30 minutes, 4 hours, 12 hours, 24 hours and 168 hours, was performed based on the expression profiles of these differentially expressed genes using the Euclidean metric. (B) Heatmap of gene expression changes for significantly differentially expressed genes involved in cytokine-cytokine receptor interaction (KEGG pathway, adjusted $p = 0.23$), derived from the qPSC versus aPSC experiment. Hierarchy clustering of samples from 4 groups, control (black), matrigel 1 μm (blue), plastic 1 μm (burlywood) and plastic 10 μm (dark brown), based on these gene expression profiles was performed. (C) Heatmap of gene expressed changes for significantly differentially expressed genes involved in cytokine-cytokine receptor interaction (adjusted $p = 0.04$), derived from the ATRA – control time course experiment.

Supplementary Figure 15: Circulating effectorT-cells in human PDAC

Effector subsets of circulating $CD4^+$ (A) and $CD8^+$ (B) T-cells were quantified by flow cytometry in age- and sex-matched 25 un-diseased donors and 8 PDAC patients. There were no differences in the effector subsets of circulating $CD4^+$ and $CD8^+$ T-cells between donors and PDAC patients. Mann Whitney U-Test; p values are two-tailed.
(C) Representative histogram showing fluorescent intensity of CXCR4 expression in $CD8^+$ T-cell of a PDAC patient relative to isotype control.

Mann Whitney U-Test; p values are two-tailed.

Supplementary Figure 16: $CD4^+$ effector and memory subsets in human PDAC

Representative flow cytometry analysis of $CD4^+$ T-cell subsets on un-diseased donor PBMCs and PDAC patient PBMC). Viable lymphocytes were gated and selected for $CD4^+$ T-cell (not shown) and were divided into the four subsets using CD45RA and CCR7.

(A) Un-diseased donor $CD4^+$ T-cell divided into naïve, CM (central memory), EM (effector memory) and TEMRA (terminally differentiated effector memory). There are few TEMRA cells.

(B) $CD4^+$ T-cell of a human PDAC patient was divided into naïve, CM, EM and TEMRA. TEMRA cells are few and the distribution of subsets is similar to un-diseased donor $CD4^+$ T-cells

(C) $CD4^+$ T-cell of a human PDAC patient with bacterial infection. Distribution of T-cell subsets differ from figures A and B with an increase in TEMRA cells observable.

Supplementary Figure 17: $CD4^+$ helper T-cell migration from PDAC patients.

(A) $CD4^+$ T-cells were measured for CXCR4 expression in age-matched normal donors (n= 6) and PDAC patients (n= 5) using flow cytometry. CXCR4 expression was significantly upregulated in PDAC patients compared to normal donors. Unpaired T-test. ** p= 0.001 to 0.01.

(B) $CD4^+$ T-cells isolated from PDAC patients were used in migration assays as described earlier. $CD4^+$ T-cells preferentially migrated to activated PSC over quiescent and to recombinant CXCL12 (positive control) over RPMI 10%. *** p< 0.001; ** p= 0.001 to 0.01; * p= 0.01 to 0.05. Comparisons were conducted with ANOVA with comparisons between columns using Bonferroni's Multiple Comparison Test.

Supplemental Figures
Supplementary Figure 1
Click here to download Supporting Document: CD8 supp figure 230613.pdf

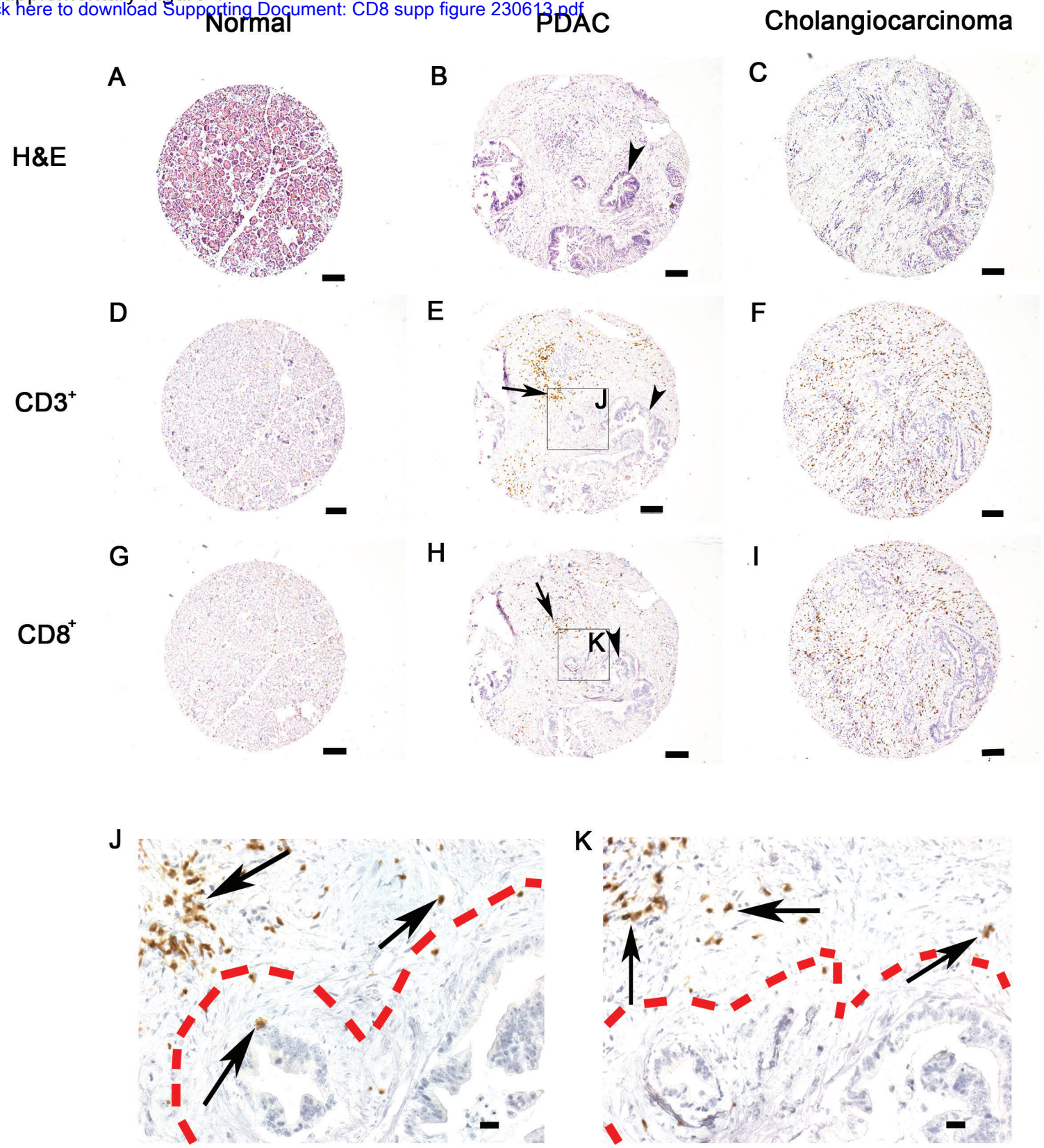

Supplementary Figure 2

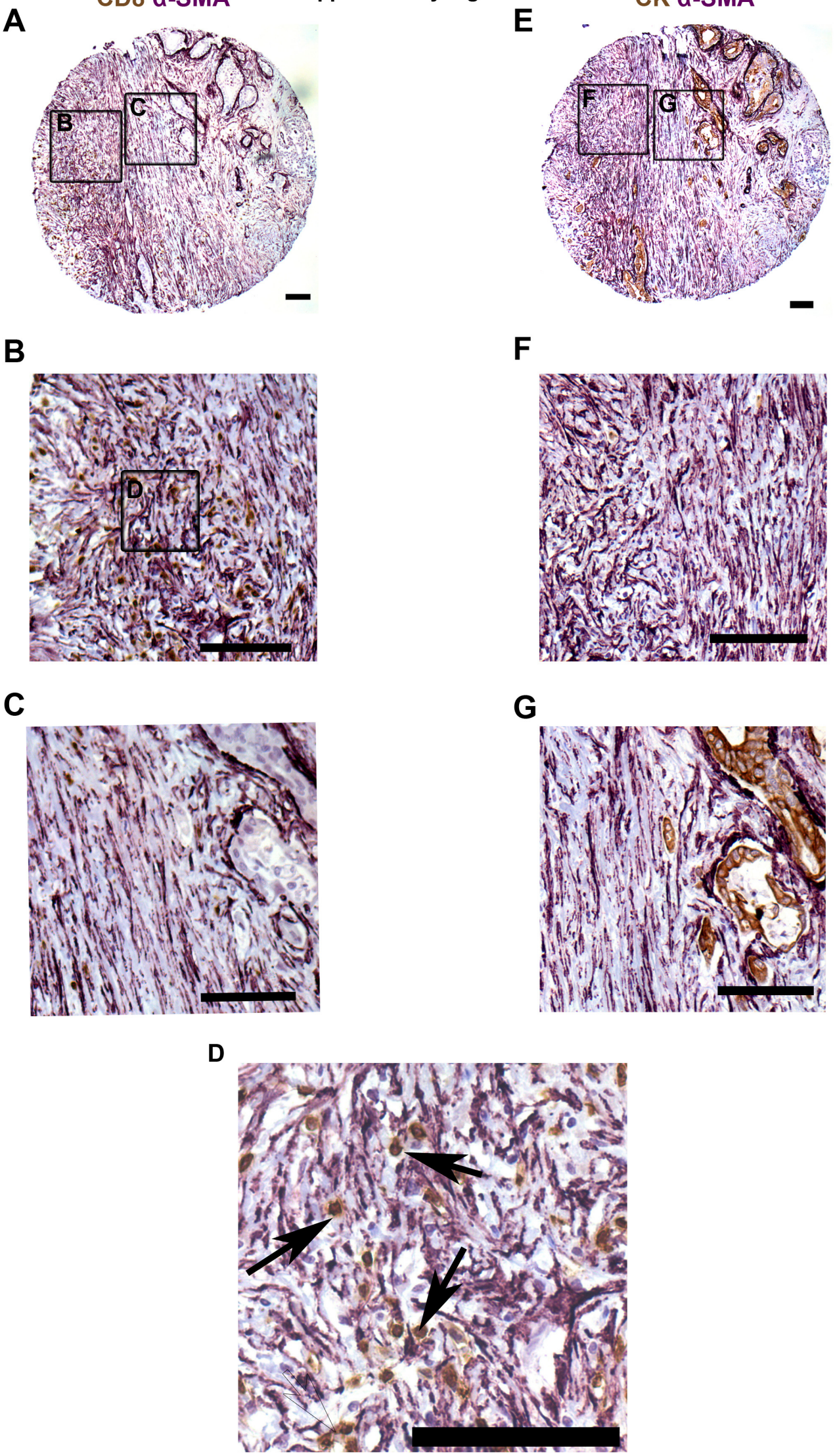

Supplementary Figure 3

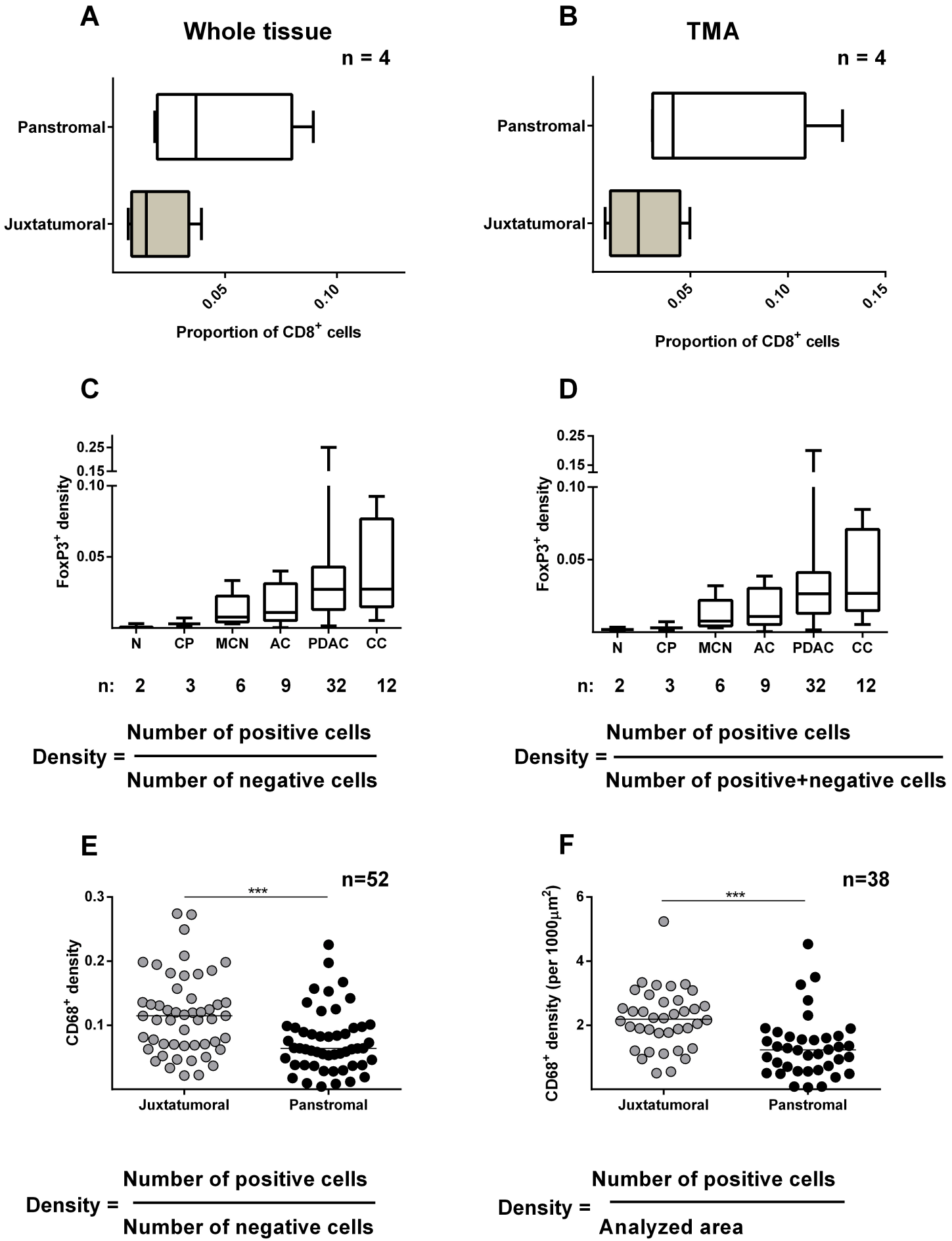

Supplementary Figure 4

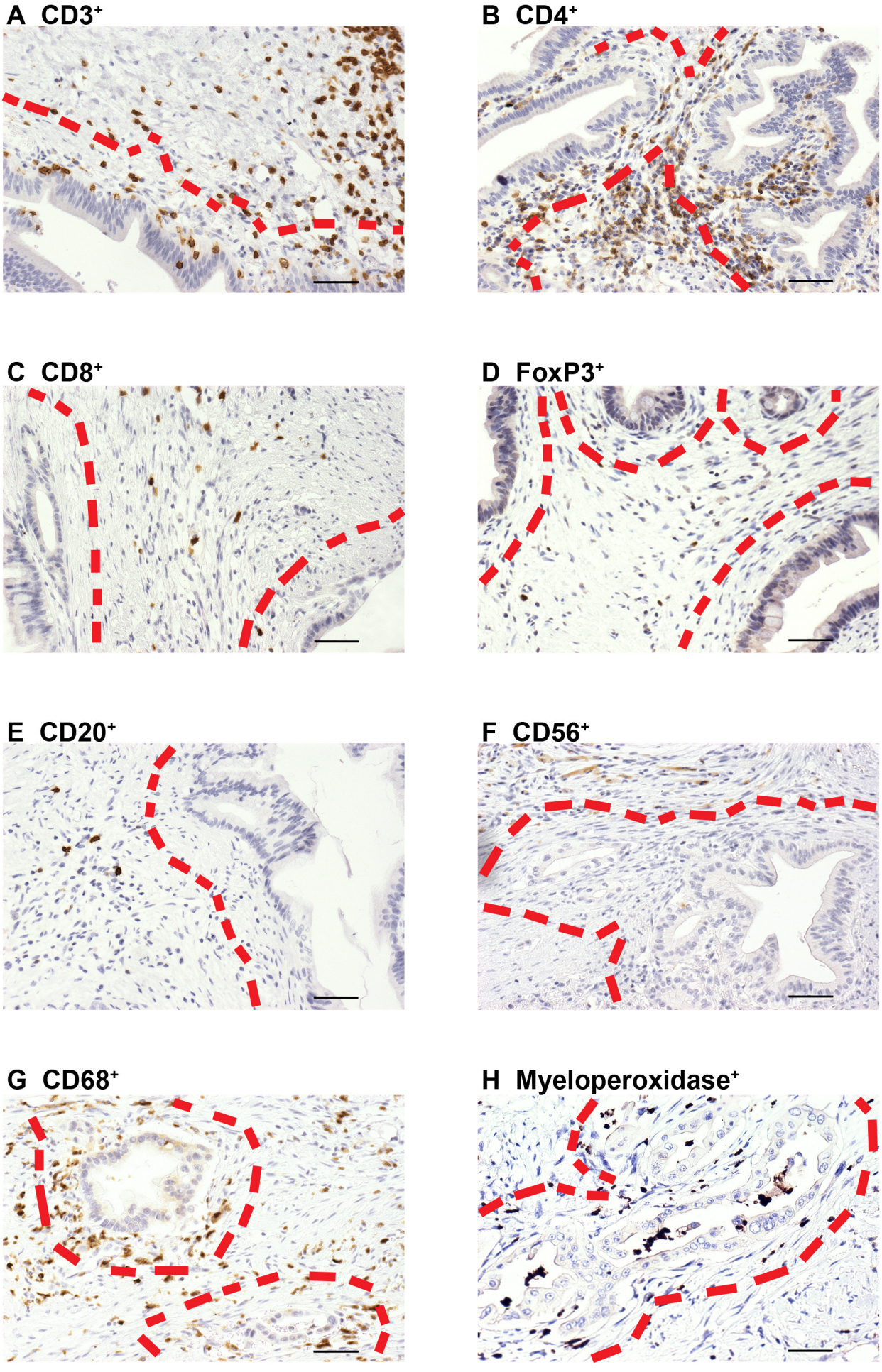

Supplementary Figure 5

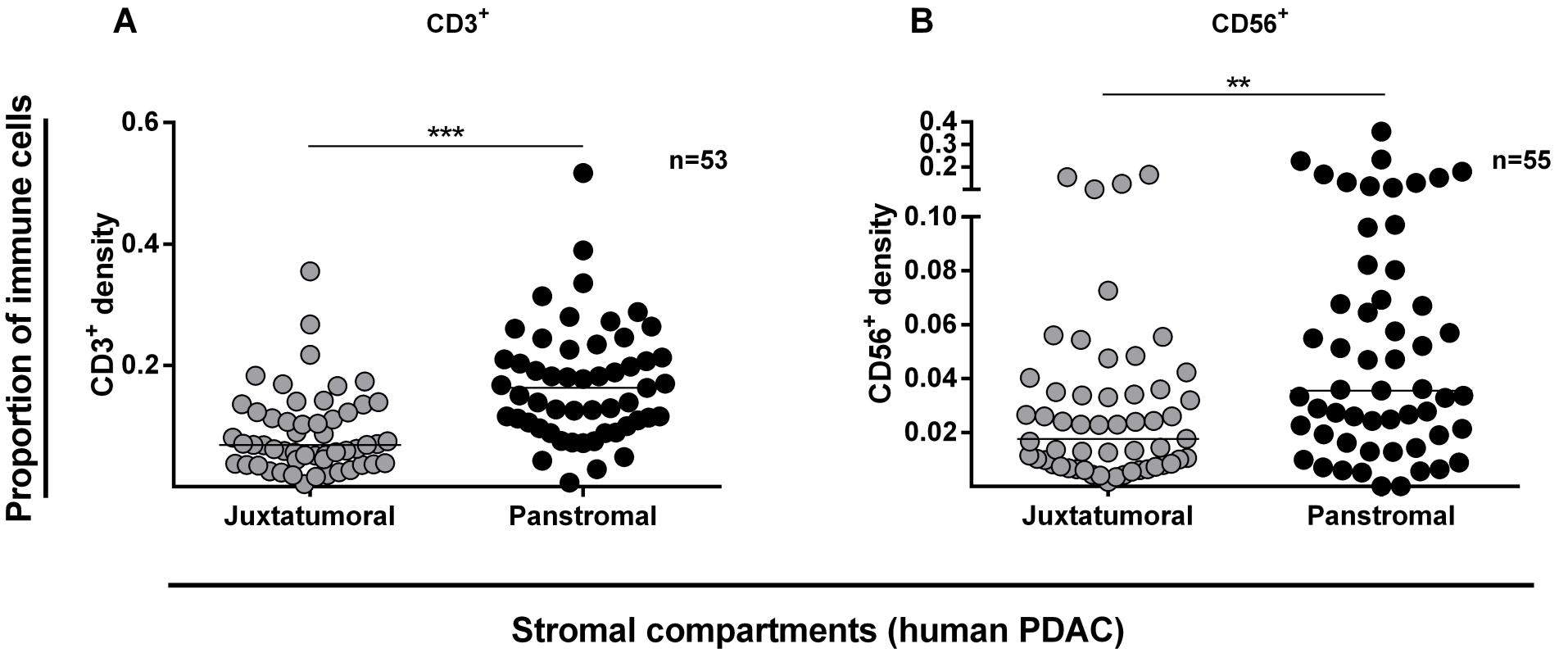

Supplementary Figure 6

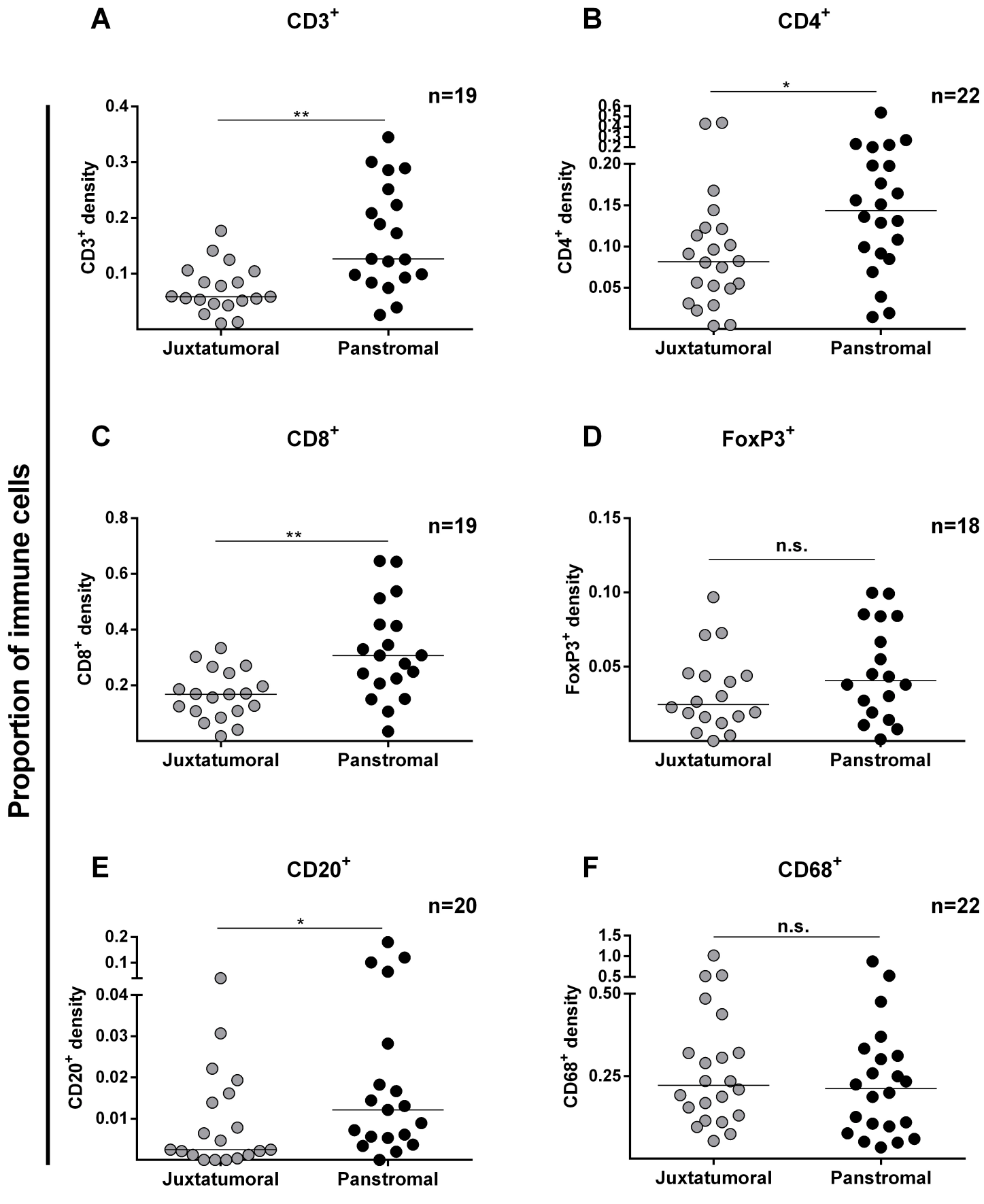

Supplementary Figure 7

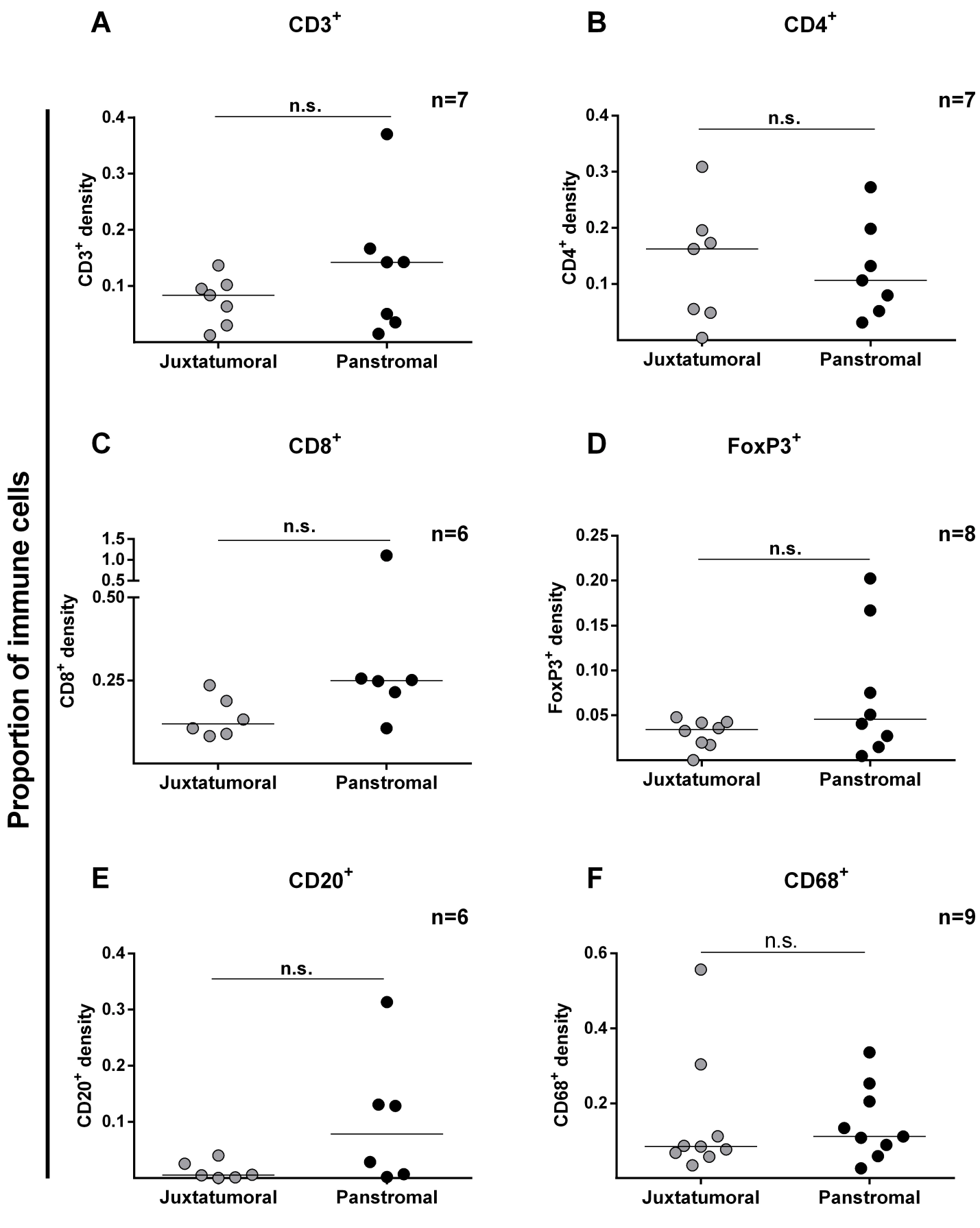

Supplementary Figure 8

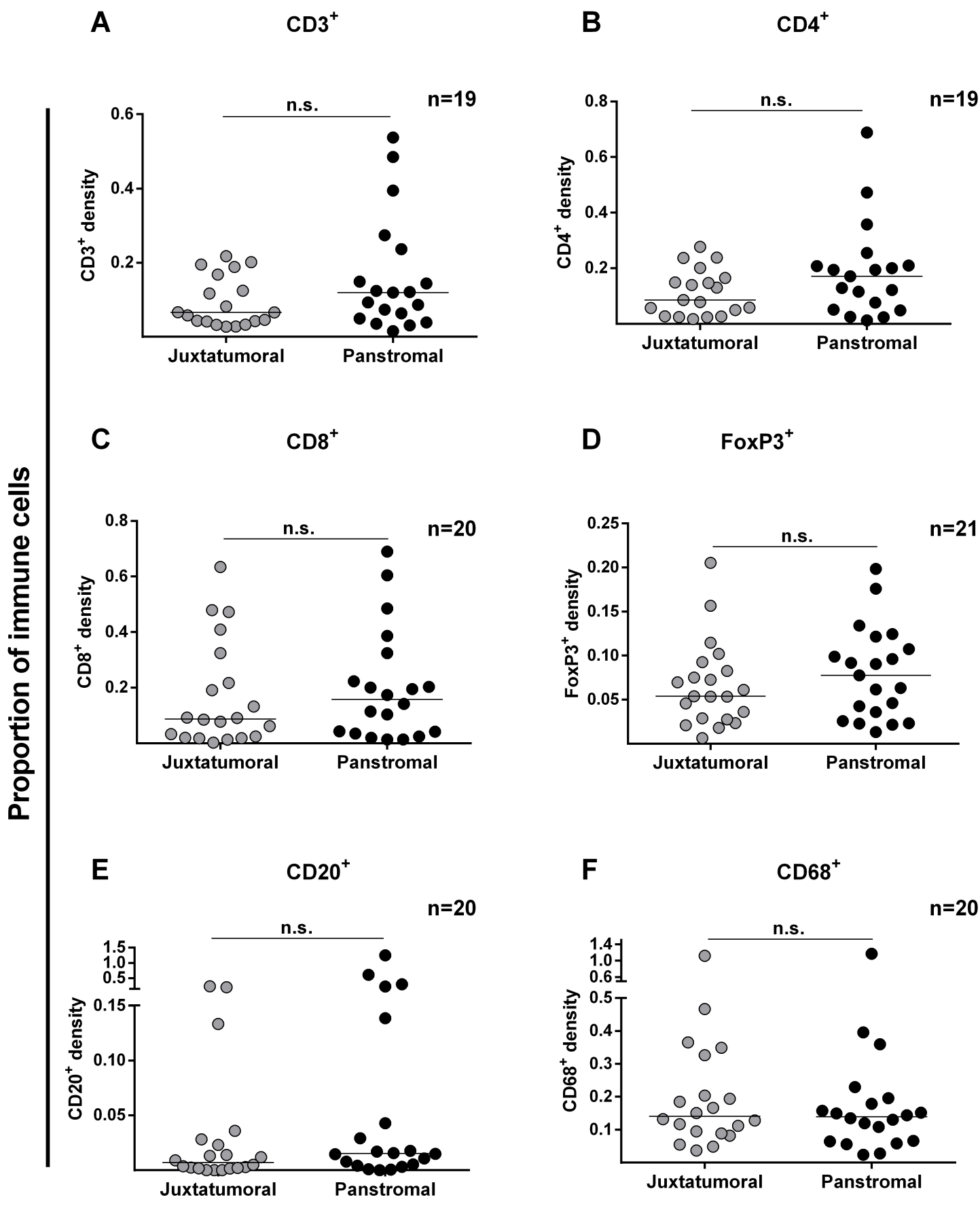

Supplementary Figure 9

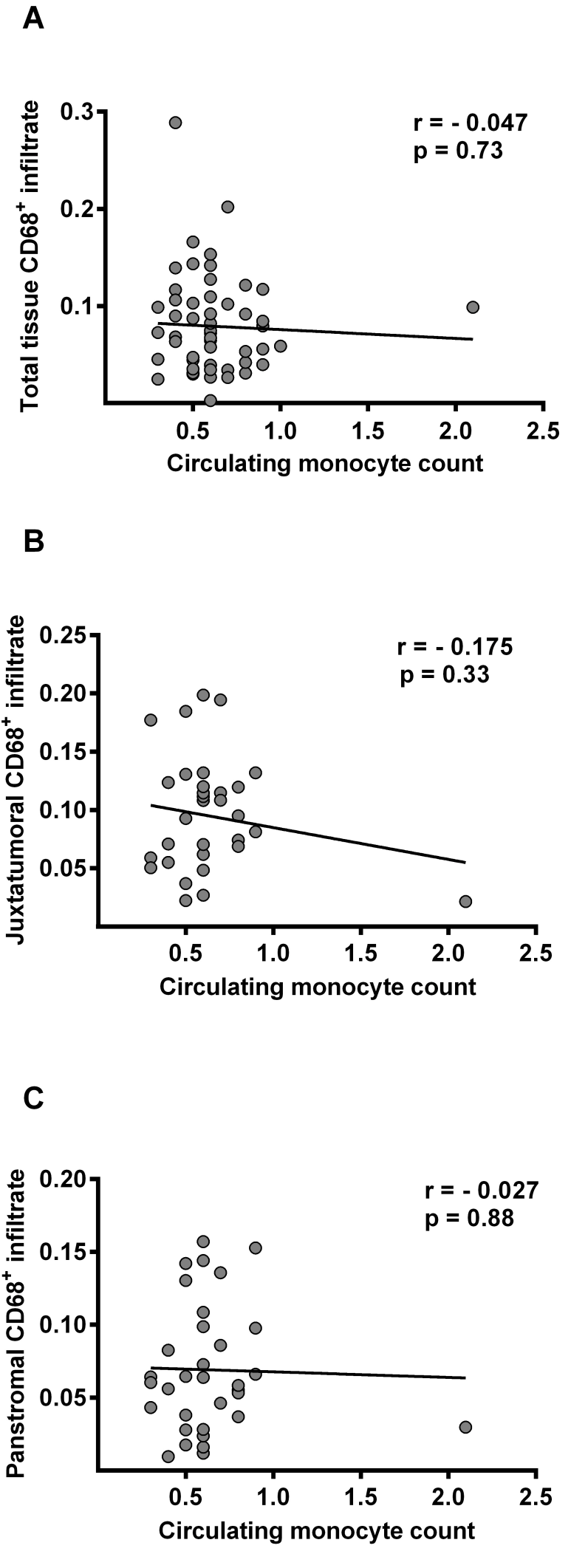

Supplementary Figure 10

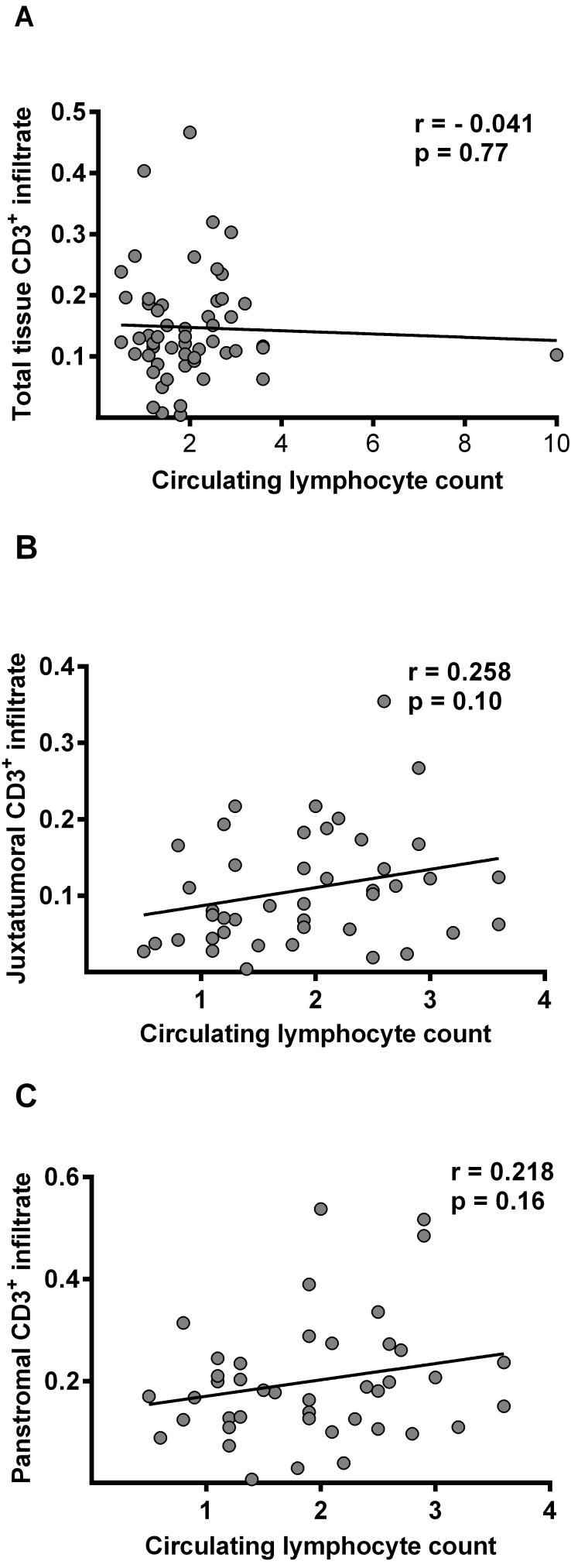

Supplementary Figure 11

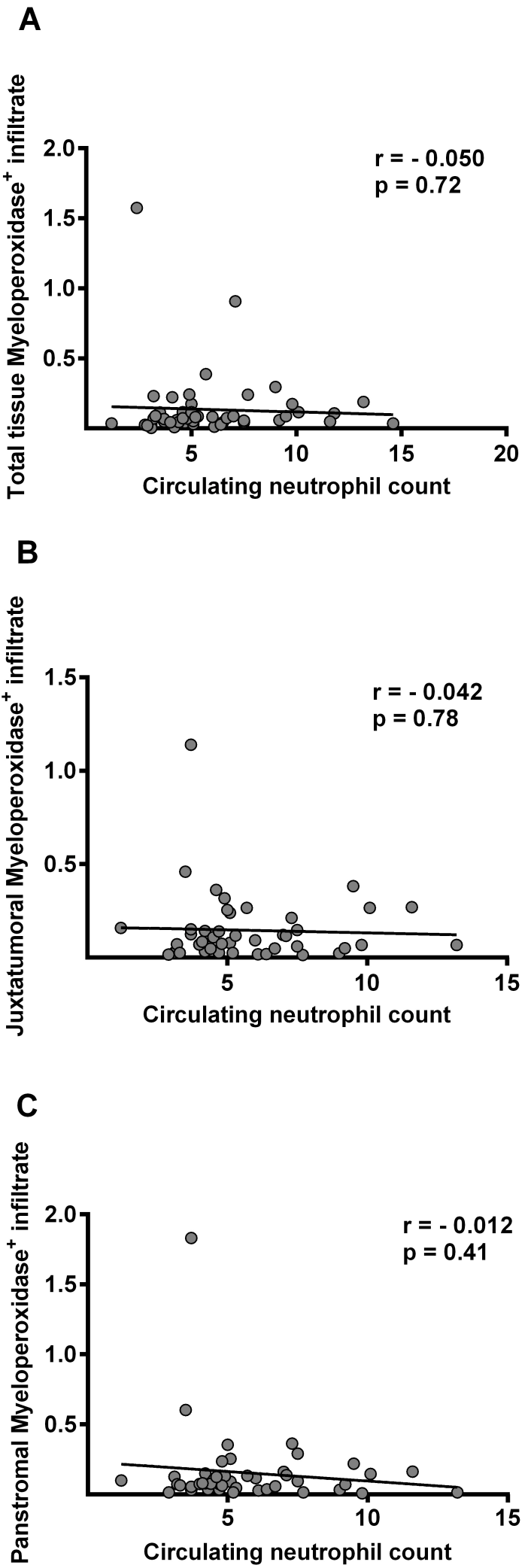

Supplementary figure 12

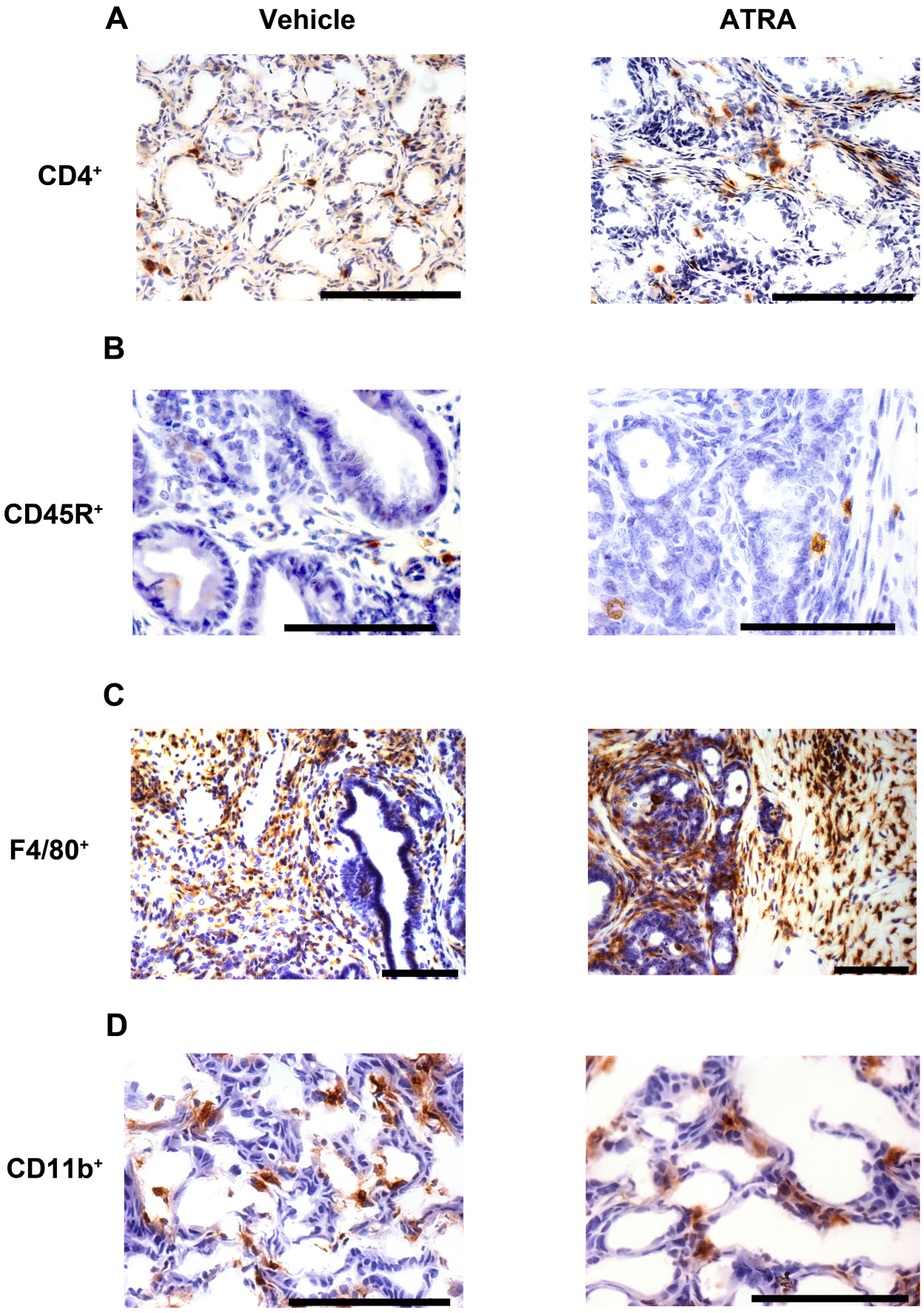

Supplementary Figure 13

A Absolute migrated cell numbers

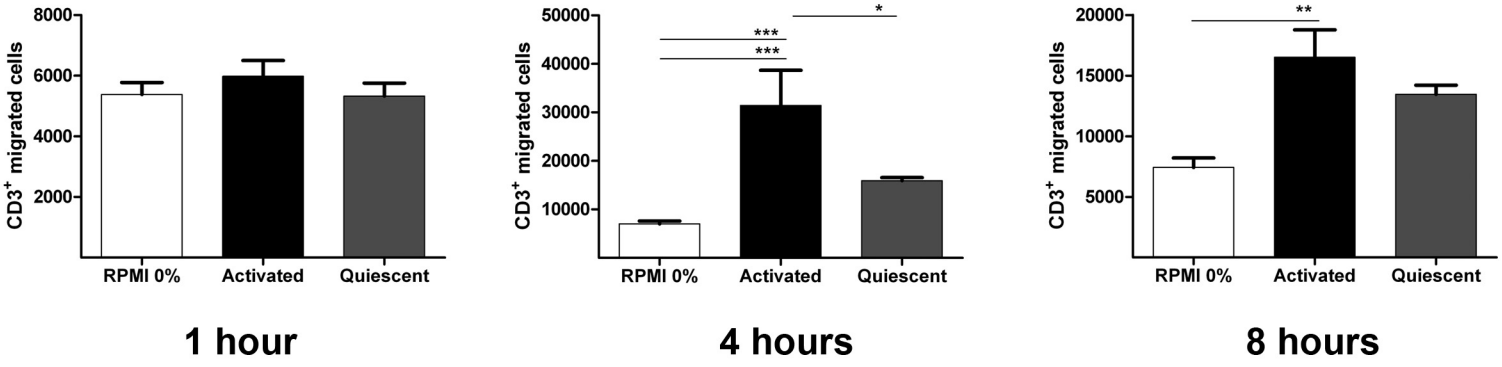

B Proportion of migrated cells

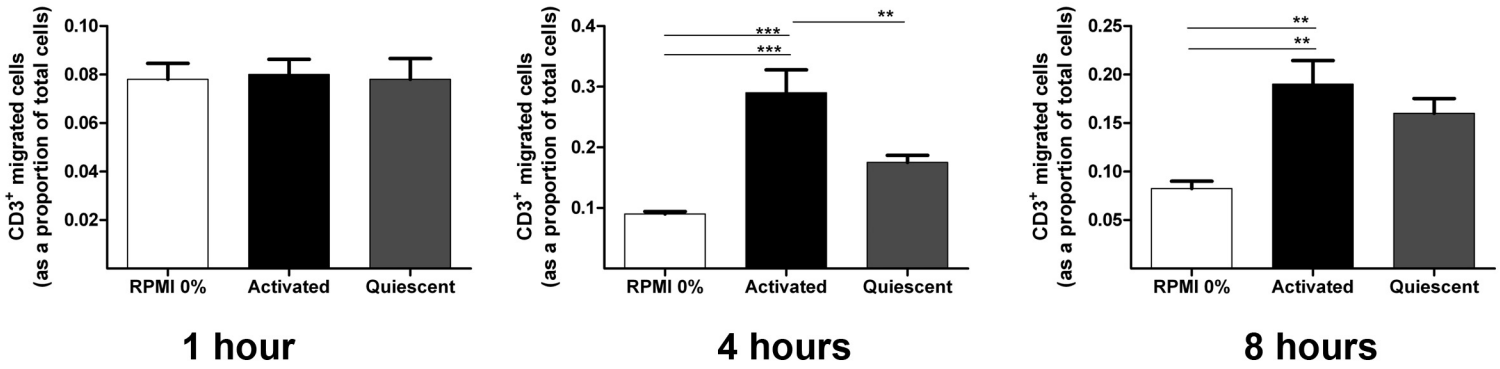

C Absolute migrated cells

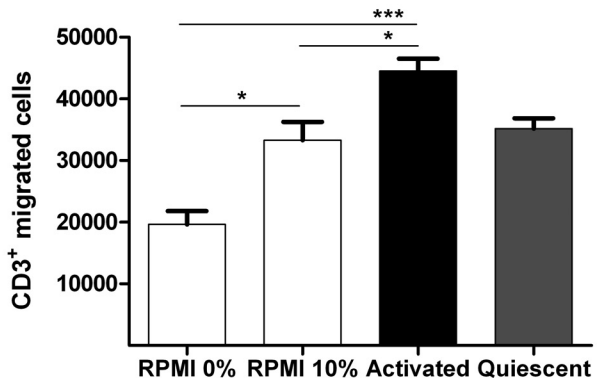

D Migrated cell number after adjustment for background migration

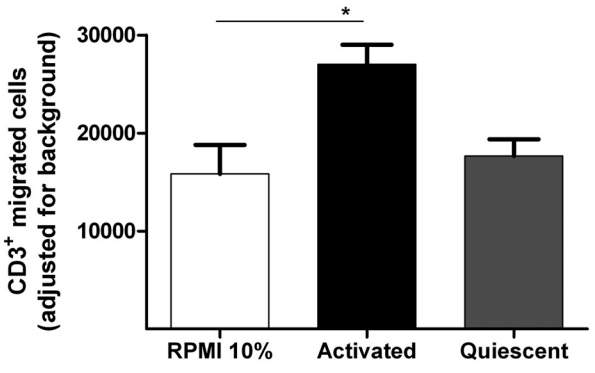

E Normalised migration

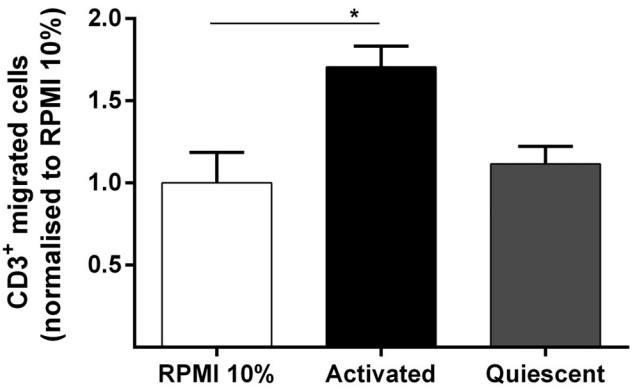

Supplementary Figure 14

A **Cell adhesion (Gene ontology: 0007155)**

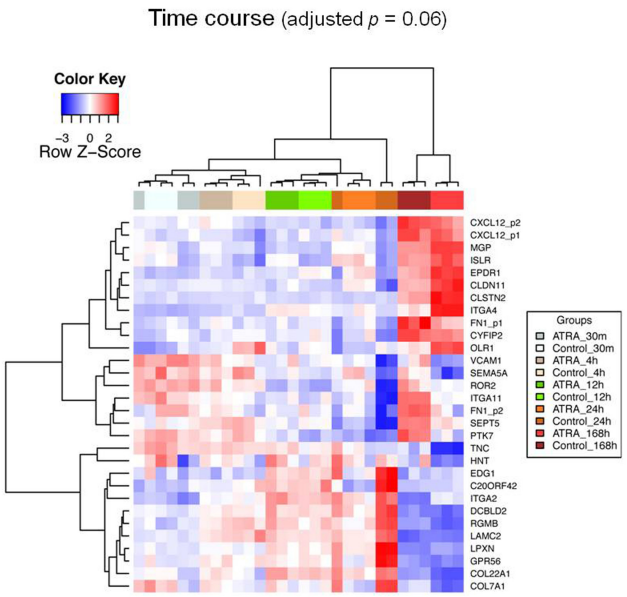

B **Cytokine-cytokine receptor interaction (KEGG pathway)**

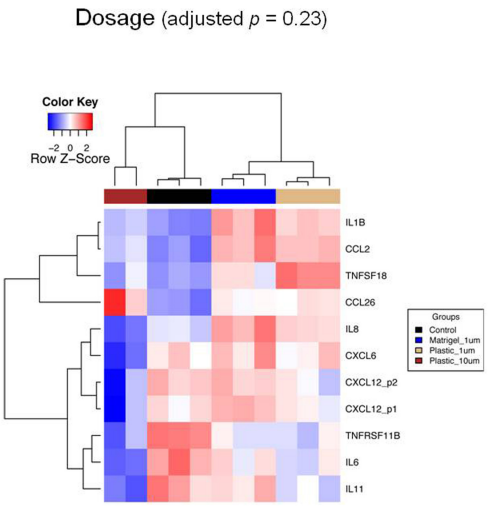

C **Cytokine-cytokine receptor interaction (KEGG pathway)**

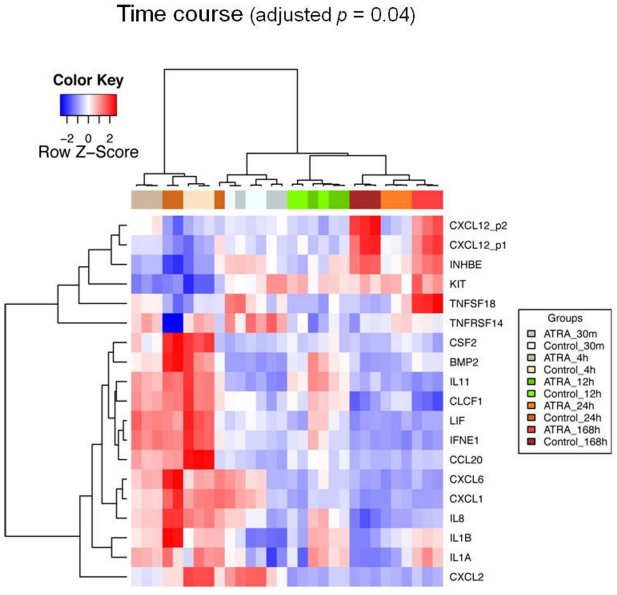

Supplementary Figure 15

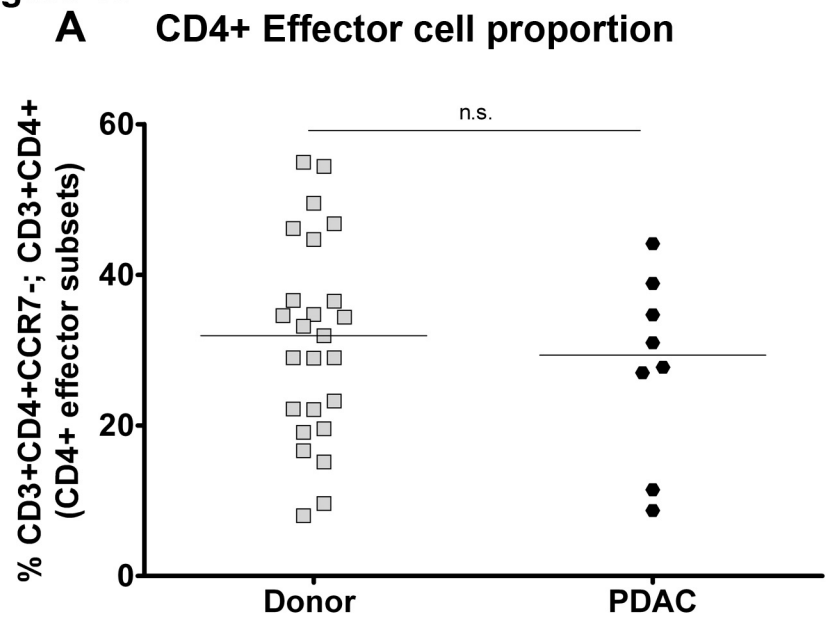

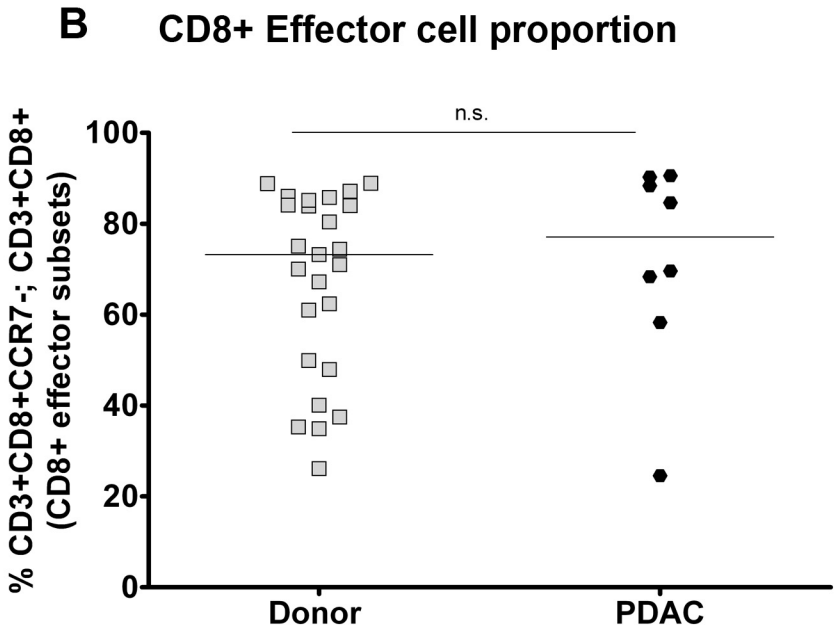

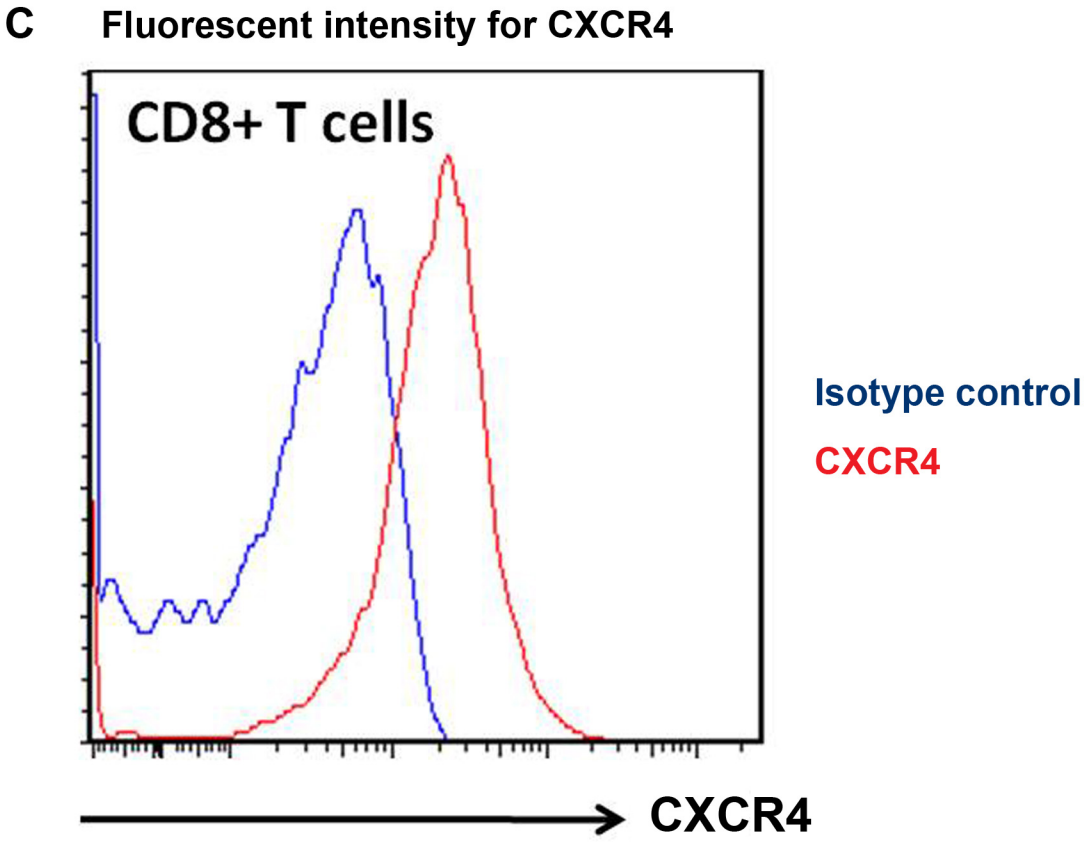

Supplementary Figure 16

CD4⁺ T-cells

A **Donor**

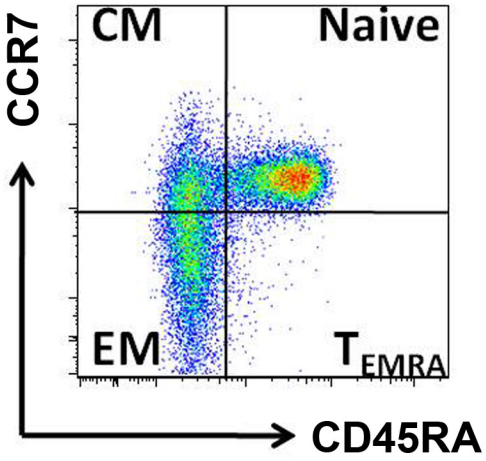

B **PDAC patient**

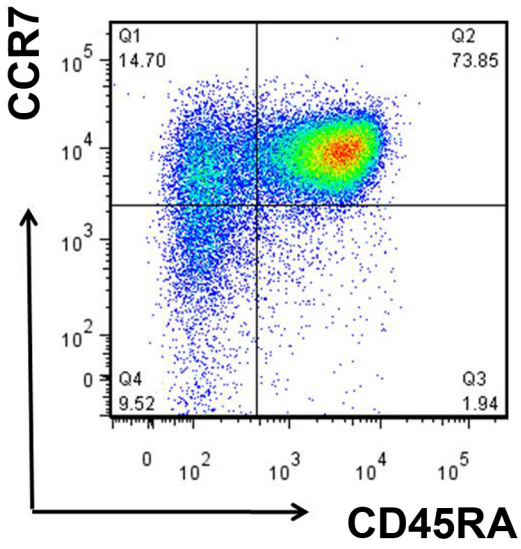

C **PDAC patient (bacterial infection)**

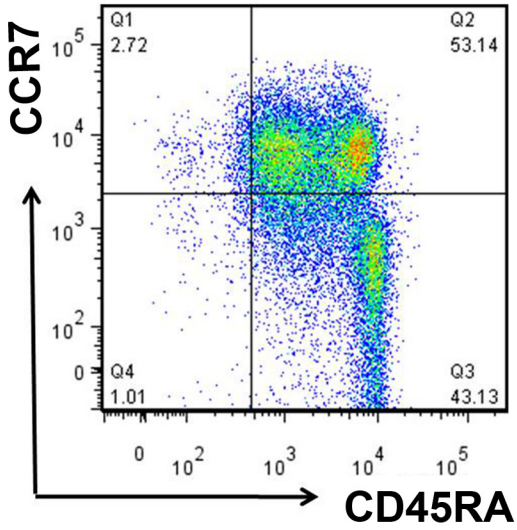

Supplementary Figure 17